Hindawi
International Journal of Antennas and Propagation
Volume 2018, Article ID 9142367, 14 pages
https://doi.org/10.1155/2018/9142367

*Research Article*

# Channel Characterization and Path Loss Modeling in Indoor Environment at 4.5, 28, and 38 GHz for 5G Cellular Networks

**Mohammed Bahjat Majed**,[1,2] **Tharek Abd Rahman**,[1] **Omar Abdul Aziz**,[1] **Mohammad Nour Hindia**,[3] **and Effariza Hanafi**[3]

[1]*Wireless Communication Center (WCC), Faculty of Electrical Eng, Universiti Teknologi Malaysia (UTM), Johor, Malaysia*
[2]*College of Science and Technology, University of Human Development (UHD), Assulaymaniyah, KRG, Iraq*
[3]*Department of Electrical Engineering, Faculty of Engineering, University of Malaya, 50603 Kuala Lumpur, Malaysia*

Correspondence should be addressed to Mohammed Bahjat Majed; mohammed.majed@uhd.edu.iq

Received 21 March 2018; Accepted 5 August 2018; Published 20 September 2018

Academic Editor: Jaume Anguera



The current propagation models used for frequency bands less than 6 GHz are not appropriate and cannot be applied for path loss modeling and channel characteristics for frequency bands above 6 GHz millimeter wave (mmWave) bands, due to the difference of signal propagation characteristics between existing frequency bands and mmWave frequency bands. Thus, extensive studies on channel characterization and path loss modeling are required to develop a general and appropriate channel model that can be suitable for a wide range of mmWave frequency bands in its modeling parameter. This paper presents a study of well-known channel models for an indoor environment on the 4.5, 28, and 38 GHz frequency bands. A new path loss model is proposed for the 28 GHz and 38 GHz frequency bands. Measurements for the indoor line-of-sight (LOS) and non-line-of-sight (NLOS) scenarios were taken every meter over a separation distance of 23 m between the TX and RX antenna locations to compare the well-known and the new large-scale generic path loss models. This measurement was conducted in a new wireless communication center WCC block P15a at Universiti Teknologi Malaysia UTM Johor, Malaysia, and the results were analyzed based on the well-known and proposed path loss models for single-frequency and multifrequency models and for directional and omnidirectional path loss models. Results show that the large-scale path loss over distance could be modeled better with good accuracy by using the simple proposed model with one parameter path loss exponent PLE ($n$) that is physically based to the transmitter power, rather than using the well-known models that have no physical base to the transmitted power, more complications (require more parameters), and lack of anticipation when explaining model parameters. The PLE values for the LOS scenario were 0.92, 0.90, and 1.07 for the V-V, V-H, and V-Omni antenna polarizations, respectively, at the 28 GHz frequency and were 2.30, 2.24, and 2.40 for the V-V, V-H, and V-Omni antenna polarizations, respectively, at the 38 GHz frequency.

## 1. Introduction

The frequency spectrum is a valuable natural resource, which has been swiftly utilized for worldwide, regional, and national telecommunication infrastructures [1, 2]. In light of this, the World Radio Conference (WRC-15) and the International Telecommunication Union for Radiocommunication (ITU-R) have been established as the main guidelines for the worldwide spectrum allocation for the next generation of cellular systems [3]. In recent years, there has been an enormous advancement in cellular data traffic owing to the development of smartphones, tablets, and devices that deliver, oversee, convey, and save zettabytes of data annually [4–6]. Moreover, the smartphone adoption rates are markedly rising as carriers and service providers are striving to engage more clients [7, 8]. Fundamentally, the arrival of smartphones and "wireless fidelity"- (WiFi-) supported devices has expedited the growth of wireless technologies and

utilization. Nevertheless, it has formed the bottleneck in the sub-6 GHz spectrum, wherein most of these devices function [9–12].

From the beginning of the 2000s, there has been an extensive utilization of 2.4 GHz and 5 GHz WiFi bands for indoor wireless communications in common workplace settings, eateries, and lodging houses [13, 14]. Nonetheless, the heavy deployment of indoor hotspots and latest wireless multimedia devices has caused high bottleneck and traffic over indoor networks [15, 16]. Moreover, the 60 GHz mmWave band is applied for wireless gigabit alliance (WiGig) along with the 2.4 GHz and 5 GHz WiFi bands, to enable high-data-rate uses. As such, the broad bandwidth at 60 GHz has promoted widespread 60 GHz indoor propagation analysis to determine the essential attributes of the channel for inventing indoor wireless local area network (WLAN) systems [17]. It should be noted that the WLAN systems have potential for attaining multi-gigabit per-second throughputs [18, 19].

In general, the wireless spectrum more than 6 GHz, particularly among 30 GHz and 300 GHz, is known as the mmWave spectrum. The mmWave spectrum encompasses a substantial volume of fresh bandwidth that is rarely used. Nevertheless, it could be feasible for unlicensed or licensed utilization in the near future [9, 10, 20]. Presently, the unlicensed 60 GHz band is the only millimeter wave band applied for extensive commercial utilization. In this case, oxygen absorption generates loss larger than free space in comparison with the alternative millimeter wave bands. Consequently, this lowers the signal strength across the extended array (up to a few hundreds of meters) of propagation distances [21].

The band more than 6 GHz at the millimeter wave band is currently purposed as a promising candidate for the latest cellular 5G communication system [22]. Accordingly, the system capability of the 5G cellular communication system will be enhanced. Consequently, the cellular devices functioned through the base station provided with an enhanced service setting with high-speed broadband transmission with low latency compared to the existing cellular communication systems [23]. Hence, the utilization of millimeter wave bands for the 5G cellular communication system will lead to innovative multimedia facilities.

Extensive characterization and modeling are required in mmWave frequency bands to obtain a general model. This study is aimed at investigating the channel characterization and path loss modelling in frequency bands below and above 6 GHz. Extensive indoor propagation measurements were performed for the 4.5, 28, and 38 GHz frequency bands. Also, a new path loss model is proposed for 28 and 38 GHz. A measurement campaign was carried out for line-of-sight (LOS) and non-line-of-sight (NLOS) scenarios to provide accurate comparisons of the well-known and new large-scale path loss models. Propagation modelling and channel characterization were investigated based on the well-known and proposed path loss models of single-frequency and multifrequency models and for directional and omnidirectional path loss models.

The rest of the paper is organized as follows. Section 2 and Section 3 discuss the recent related work and the measurement environment and experiment procedures, respectively. Section 4 presents measurement hardware equipments. Large-scale characterization for single-frequency and multifrequency path loss models is presented in Section 5. The proposed model is provided in Section 6. Section 7 presents measurement results and discussion. The proposed model analysis is discussed in Section 8. Finally, the conclusions of the results are provided in Section 9.

## 2. Related Work

Over the past 25 years, many studies have focused on the indoor propagation and channel modelling for a frequency less than 6 GHz. For example, a 900 MHz signal using 200 kHz of bandwidth had attenuation between 28 dB and 61 dB per decade of distance for a radius up to 27 m. The experiment was conducted in multiple floors of an indoor workplace setting [24]. Using a similar setting, another study demonstrated attenuation about 31 dB at $d_0 = 1\ m$ (FSPL in the first meter) at 900 MHz with four breakpoints. The study utilized a multiple slope model at larger distances and PLE value of 2 for a radius up to 10 m [25]. Furthermore, an indoor multipath propagation analysis was conducted by Saleh and Valenzuela. The study was conducted at 2 m heights via a 10-nanosecond (ns) probing pulse positioned at 1.5 GHz with V-V polarization discone antennas for the transmitter and receiver [26]. The indoor channel had the attenuation of signal per decade, ranging from 30 dB to 40 dB.

In the beginning of the 1990s, Rappaport et al. employed circularly and linearly polarized antennas for indoor analysis at 1.3 GHz and 4 GHz. The findings demonstrated a similar propagation path loss for 1.3 GHz and 4 GHz and greater cross-polarization discrimination for LOS channels in comparison with NLOS or blocked channels [27, 28]. Subsequently, the importance of applying a 1 m reference radius aiming at significant indoor path loss models was reported [29]. The authors also indicated the practicability of ray-tracing in terms of estimating the impulse response of indoor channels for single-floor and multifloor propagation. A household structure exhibited PLE values of 1.7 and 3.1 for LOS and NLOS at the 5 GHz frequency, with respect to the 1 m open-space reference radius [30]. In addition, analysis of indoor workplaces using soft dividers at 900 MHz and 1900 MHz demonstrated PLE values of 2.4 and 2.6, respectively (w.r.t.), and a 1 m free-space reference distance constituting standard deviations of 9.6 dB and 14.1 dB, respectively. Furthermore, a radiofrequency infiltration for metallic shaded windows revealed attenuation ranging from 3 dB and 30 dB. Moreover, Rappaport and Sandhu demonstrated an analysis on signal propagation for a wide range of frequencies from 850 MHz to 60 GHz. Moreover, the study investigated signal propagation for wireless communications systems within buildings [31].

Also prior to the beginning of the 1990s, there have been numerous investigations focused on mmWave bands intended for the indoor setting. These studies mainly focused on the 60 GHz band, which is the furthermost potential approach for multi-gigabit wireless indoor communications systems. An open-ended waveguide at the transmitter and

directional horn antenna at the receiver were used for analysis of indoor channels at 60 GHz [18, 32]. A sliding correlator channel sounder was utilized with an RF null-to-null bandwidth of 200 MHz and a 10 ns time resolution, with power delay profiles (PDPs) or channel impulse responses captured at discrete pointing angles while rotating the receiver antenna. LOS analysis with a 1 m close-in free-space reference distance revealed a PLE value below 2 (theoretical FSPL). The results were equivalent with lesser frequencies in indoor settings.

A rotated horn antenna was employed for indoor laboratory analysis at 28 GHz, where VNA was used to quantify the channel [33]. The authors utilized the Saleh-Valenzuela model to describe the indoor channel. Moreover, a study used a VNA and a pair of horn antennas with a 26 dBi gain and 30 m distance range for propagation analysis in an indoor setting at the 28 GHz channel. The PLE in various indoor settings was expected to be 2, 2.2, 1.2, and 1.8 in a free space, hallway, corridor, and office, respectively [34]. In addition, reflection and penetration loss analysis was performed at 28 GHz inside and nearby buildings in New York City [35]. The findings demonstrated a huge penetration loss of 45.1 dB for an office building with three interior walls. Also, outdoor tinted glass caused a penetration loss of 40.1 dB compared to indoor nontinted glass that had 3.9 dB of penetration loss. A measurement was conducted [36] in an anechoic chamber and in the laboratory on the 28 and 82 GHz frequency bands to characterize the channel in the mmWave bands. Hindia et al. conducted a measurement to study a well-known channel model in an outdoor environment on 26, 28, 36, and 38 frequency bands for single-frequency and multifrequency schemes, and they also propose a new path loss model for the outdoor environment [37]. In [38–40], measurements were conducted at 28 and 73 GHz frequency bands in an indoor office using directional and omnidirectional antennas. In these studies, the large-scale and small-scale parameters were characterized. In [41, 42], measurements and simulation were conducted at the 28, 38, and 73 GHz frequency bands to characterize the propagation channel in CI and ABG path loss models and to evaluate and estimate some parameters.

## 3. Measurement Environment and Experiment Procedures

Quantifications at the 4.5, 28, and 38 GHz carrier signals were conducted to generate a prototype of the 5G wireless links that proposed to function through prospective 5G network bands. Measurement campaigns were conducted with reference to LOS and NLOS case studies. These campaigns resemble the access communication links among the base and mobile stations for upcoming mobile networks. The measurement was conducted in the ground floor of a two-storey structure, namely, new wireless communication center WCC block P15a, which is located in Universiti Teknologi Malaysia UTM Johor, Malaysia. The building is built on external concrete walls, while all the internal walls between the rooms are constructed using glass and gypsum board with thickness around 5 cm. Moreover, it has glass and wooden doors plus clear glass internal and external windows. Also, the structure has workplace settings and laboratories with typical blocks like workspace, chairs, corridor, doors, cubicle dividers, lobbies, offices, and classrooms.

TX and RX horn antennas were vertically polarized (V-V) for copolarization assessments of directional path loss models. Meanwhile, the TX antenna was vertically polarized, and the RX antenna was horizontally polarized (V-H) for the cross-polarization assessments. Furthermore, the TX horn antenna and RX omni antenna were both vertically polarized for the omnidirectional path loss model. Essentially, TX height was established at 2 m overhead the ground level, where it is assumed as an indoor hotspot on the wall. Meanwhile, the height of the RX antenna was fixed at 1.5 m (usual handset height) and the ceiling height is 2.7 m.

The quantifications of power were performed through choosing 1 TX site and 33 RX sites in the building. Moreover, all RX sites are scattered among LOS and NLOS with the distances of TX-RX separation extending between 1 m and 22.7 m. It should be noted that the ground floor dimensions were approximately 21 m × 30 m. The resulting zero-point distance between the transmitter and receiver was 1 m (i.e., first point of the assessment). The 16 LOS assessment sites required 3D distances between 1 m and 14 m. Meanwhile, 17 NLOS assessment sites required 3D distances between 12 m and 22.7 m.

For the assessment procedure, firstly, the TX antenna was positioned at an immovable location in the corridor of the ground floor of the building as demonstrated in Figure 1. The assessment was commenced with the RX 1 m from the transmitter, where the received signal was documented along with the RX stationary at that location. Subsequently, the Rx was relocated 1 m apart from the TX. Moreover, the stationary quantifications were re-ran for all 33 RX sites. Moreover, TX and RX antennas were positioned in the azimuth and elevation planes, where PDPs were documented.

## 4. Measurement Hardware Equipments

In the vicinity of the TX side, an Anritsu MG369xC Series Synthesized Signal Generator device was utilized to produce continuous radiowave signals; the output of the radiofrequency was linked to an extremely directional horn antenna with a vertical polarization. In the vicinity of the RX side, the received power level was quantified through linking the vertically/horizontally polarized horn antenna and omni antenna to the MS2720T high-performance handheld spectrum analyzer. It was functioned at zero spans, and the channel bandwidth of the spectrum analyzer was fixed at 100 kHz. If TX and RX were both horn antennas for the entire frequencies, the transmitted power $P_t$ of the signal was 10 dBm. Meanwhile, if the RX was an omni antenna, the transmitted power was 25 dBm. This is due to the gain of the omni antenna, which was 3 dBi. Table 1 illustrates the assessment setup factors of all quantified frequencies.

## 5. Large-Scale Characterization

The path loss is the key factor utilized to characterize the large-scale impacts of the propagation channel as for the


Figure 1: Measurement environment at (new WCC) block P15a-UTM.

Table 1: Assessment setup factors.

| | | | |
|---|---|---|---|
| Carrier frequency (GHz) | 4.5 | 28 | 38 |
| Transmit power (dBm) | | 10, 25 | |
| TX horn antenna gain (dBi) | 10.0 | 19.2 | 21.1 |
| RX horn antenna gain (dBi) | 10.0 | 19.2 | 21.1 |
| RX omni antenna gain (dBi) | | 3 | |
| TX height (m) | | 2 | |
| RX height (m) | | 1.5 | |
| Polarization of TX | | Vertical | |
| Polarization of RX | | Vertical/horizontal | |

received signal. The path loss determines the large-scale fading behavior with reference to power attenuation as a function of distance and frequency [43, 44].

*5.1. Single-Frequency Path Loss Models.* The close-in (CI) free-space path loss model is a well-known path loss model [45]. In general, the path loss model is applied to demonstrate the impacts of the channel induced in virtue of the adjacent setting. The path loss model evaluates the power attenuation parameter, which is referred to as the fading behavior being a function of distance and frequency. The close-in (CI) free-space path loss model is denoted as follows (1) [45]:

$$\mathrm{PL}^{\mathrm{CI}}(f,d)[\mathrm{dB}] = \mathrm{FSPL}(f,d_0) + 10_n \log_{10}\left(\frac{d}{d0}\right) + X\sigma^{\mathrm{CI}}, \tag{1}$$

where $n$ represents the PLE, $X\sigma^{\mathrm{CI}}$ represents a Gaussian random variable, $\sigma$ symbolizes the standard deviation in dB, and $d_0 = 1$ m indicates the physical reference distance [29, 46].

The floating-intercept (FI) path loss model is also a type of path loss model, which is applied in WINNER II and 3GPP standards [46, 47]. FI is relied upon the FI ($\alpha$) and the line slope ($\beta$) to achieve the best minimum error fit of the composed path losses. The FI is denoted as

$$\mathrm{PL}^{\mathrm{FI}}(d)[\mathrm{dB}] = \alpha + 10.\beta \log_{10}(d) + X_\sigma{}^{\mathrm{FI}}, \tag{2}$$

where $\alpha$ represents the floating intercept in dB, $\beta$ indicates the line slope, and $X_\sigma{}^{\mathrm{FI}}$ symbolizes the large-scale signal variabilities received against the distance in the direct path.

*5.2. Multifrequency Path Loss Model.* The alpha-beta-gamma (ABG) model is an important multifrequency path loss model. Commonly, multifrequency path loss models are needed to normalize the path loss models to cover a broad spectrum of frequencies. As such, this is determined by frequency and distance. In light of this, previous studies have demonstrated the multifrequency model plus the three parameter models [48, 49]. Hence, the equation of the ABG model is expressed as

$$\mathrm{PL}^{\mathrm{ABG}}(f,d)[\mathrm{dB}] = 10\alpha \log_{10}\left(\frac{d}{d_0}\right) + \beta + 10\gamma \log_{10}\left(\frac{f}{f_0}\right) + \chi_\sigma^{\mathrm{ABG}}, \tag{3}$$

where $\alpha$ and $\gamma$ represent the path loss coefficients that characterize the distance and frequency dependency, respectively, $\beta$ indicates the path loss optimized offset, $f$ denotes the operation frequency (GHz), $f_0$ represents a fixed reference frequency, and $X_\sigma{}^{\mathrm{ABG}}$ symbolizes the large-scale signal variabilities received against the distance in the direct path.

## 6. Proposed Model for 28 GHz and 38 GHz Frequency Bands

The progressing narrow-beam mmWave system can be utilized for scenarios of many angles of arrival, where receivers merge majority of the received energy. The current proposed model has simplified the system design and performance assessments. The regular single-slope path loss function was unable to capture the path loss dependence with separation distance in high-density surroundings with manifold obstructions. The proposed hybrid probabilistic path loss model can be applied as a substitute for the conventional propagation path loss models against unique TX-RX separation distances to quantify the path loss. The V-V environment is referred to as the reference for LOS scenario in both frequencies, and the V-Omni environment is referred to as the reference for the NLOS scenario in both frequencies. The path loss value is linked with distance $d$ and divided into two components such as LOS and NLOS coefficient factors. Analogous to the CI path loss model, the proposed model assessments provide physically based and efficient estimated path loss data points for the reference distance $d_0 = 1$ m. Two correction coefficients are suggested for the LOS and NLOS surroundings for the mmWave bands as demonstrated in (5), (6), and (7), respectively. $\mathfrak{I}\mathrm{LOS}(d_i)$ and $\mathfrak{I}\mathrm{NLOS}(d_i)$ in dB are anticipated to offer the good match path loss as determined by the measured data. The regular methodology for propagation models at any mmWave frequency with any antenna can be precisely examined using a standard free-space reference distance of $d_0 = 1$ m for all mmWave assessments and path loss models. The study proposed a generic propagation model through the probabilistic distributions for the LOS and NLOS circumstances as a function of the

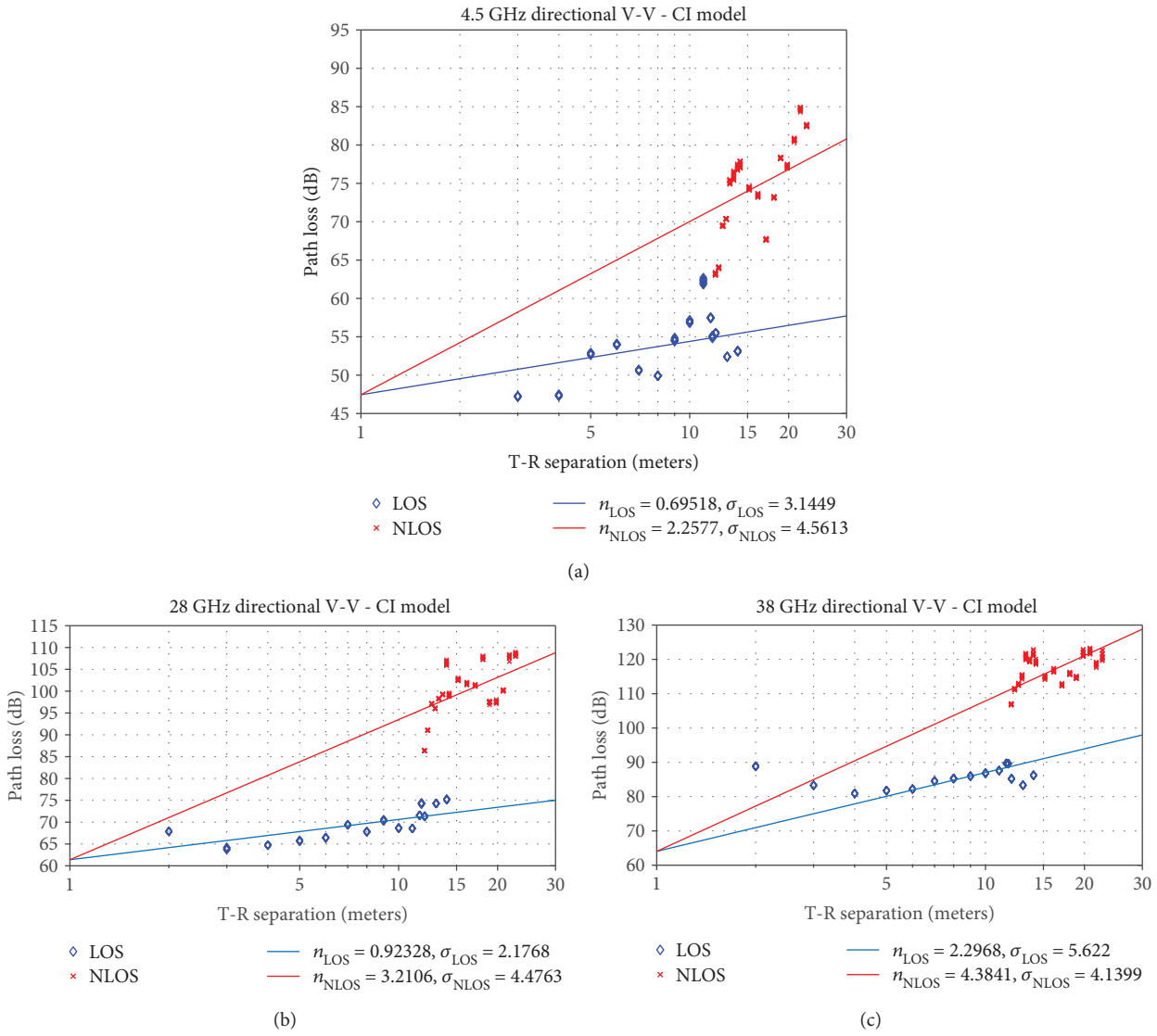


Figure 2: Directional V-V CI path loss model for LOS and NLOS (a) 4.5 GHz, (b) 28 GHz, and (c) 38 GHz.

TX-RX separation and variation of the path loss values is suggested as

$$\mathrm{PL}_{\mathrm{pro}}(f,d) = \mathrm{PL}(f,d_0) + 10n\log\left(\frac{d}{d_0}\right) + \mathfrak{F}(d_i) + X_\sigma,$$
$$\mathfrak{F}(d_i) = \begin{cases} \mathfrak{F}_{\mathrm{LOS}}(d_i), & \forall d_0 \le d \le d_{i+1}, \\ \mathfrak{F}_{\mathrm{NLOS}}(d_i), & \forall d_{i+1} \le d \le \ell, \end{cases} \tag{4}$$

where $\mathfrak{F}(d_i)$ in a (V-V) environment is

$$\mathfrak{F}_{\mathrm{LOS}}(d_i) = 0,$$
$$\mathfrak{F}_{\mathrm{NLOS}}(d_i) = \sqrt{\sum_{i+1}^{\ell}\left\{\left[\mathrm{PL}_{V-V}(f,d_i) - \mathrm{PL}_{V\text{-}\mathrm{Omni}}(f,d_i)\right]^2\right\}}, \tag{5}$$

and $\mathfrak{F}(d_i)$ in a (V-H) environment is

$$\mathfrak{F}_{\mathrm{LOS}}(d_i) = \sqrt{\sum_{i=1}^{i+1}\left\{\left[\mathrm{PL}_{V-H}(f,d_i) - \mathrm{PL}_{V-V}(f,d_i)\right]^2\right\}},$$
$$\mathfrak{F}_{\mathrm{NLOS}}(d_i) = \sqrt{\sum_{i+1}^{\ell}\left\{\left[\mathrm{PL}_{V-H}(f,d_i) - \mathrm{PL}_{V\text{-}\mathrm{omni}}(f,d_i)\right]^2\right\}}, \tag{6}$$

and $\mathfrak{F}(d_i)$ in a (V-Omni) environment is

$$\mathfrak{F}_{\mathrm{LOS}}(d_i) = \sqrt{\sum_{i=1}^{i+1}\left\{\left[\mathrm{PL}_{V\text{-}\mathrm{Omni}}(f,d_i) - \mathrm{PL}_{V-V}(f,d_i)\right]^2\right\}}, \tag{7}$$
$$\mathfrak{F}_{\mathrm{NLOS}}(d_i) = 0,$$

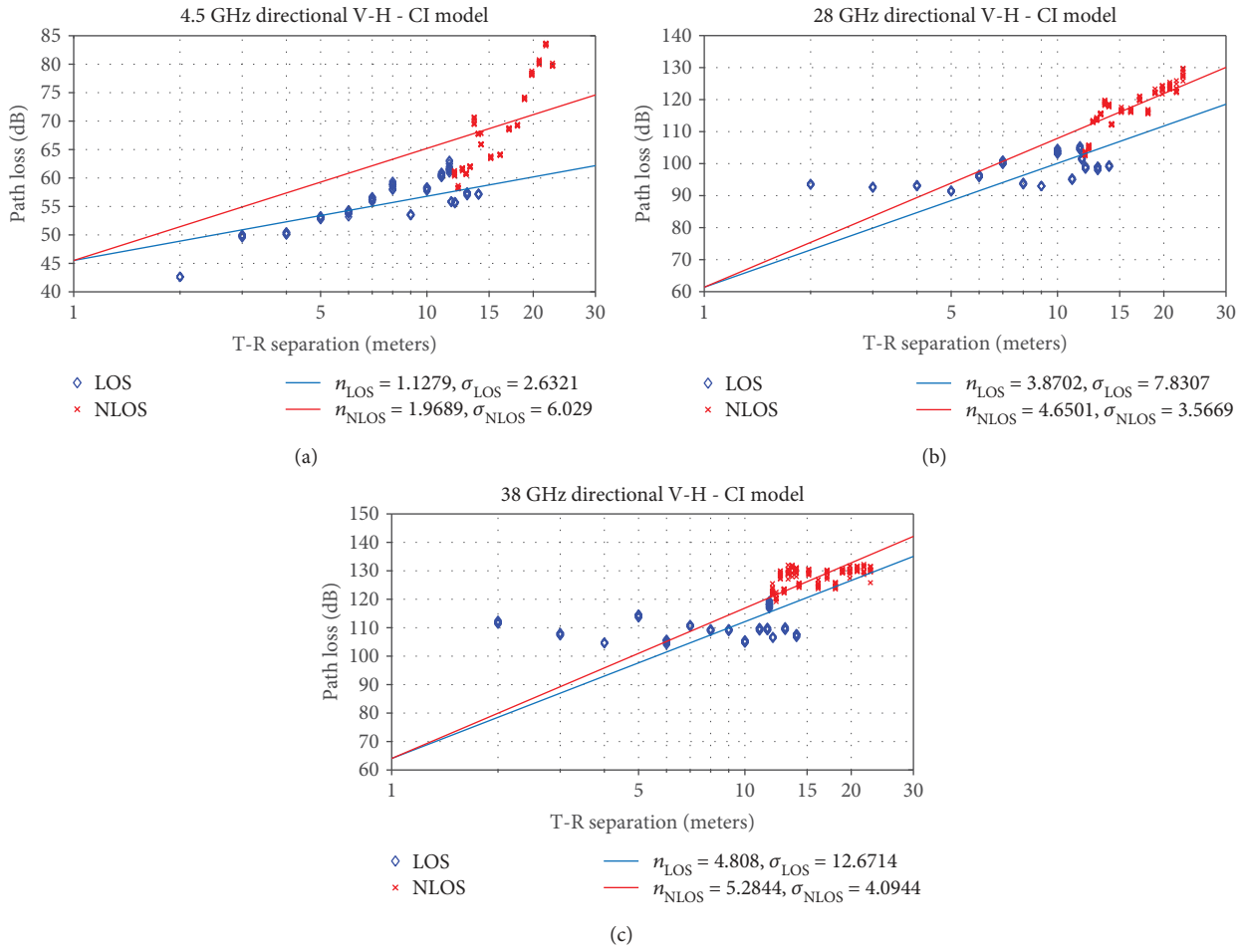


Figure 3: Directional V-H CI path loss model for LOS and NLOS (a) 4.5 GHz, (b) 28 GHz, and (c) 38 GHz.

where $\mathfrak{F}(d_i)$ represents the generic compensation function in regards to the observed environment; $\mathfrak{F}\mathrm{LOS}(d_i)$ and $\mathfrak{F}\mathrm{NLOS}(d_i)$ symbolize the combined measured points at identical separation distances for the LOS and NLOS scenarios, respectively; $\mathrm{PL}(f, d_0)$ indicates the path loss at $d_0 = 1$ m; $i$ represents the distance index; and $\ell$ indicates the maximum separation distance.

## 7. Measurement Results and Discussion

*7.1. Single-Frequency Path Loss Models.* Figures 2, 3, and 4 show the directional and omnidirectional path loss for the CI model at 4.5, 28, and 38 GHz in the LOS and NLOS environments for (V-V), (V-H), and (V-Omni) antenna polarization, respectively. For V-V antenna polarization, the PLE values in the LOS case study were 0.7, 0.92, and 2.29 at 4.5, 28, and 38 GHz, respectively. And for V-H antenna polarization, the PLE values in the LOS case study also were 1.13, 3.87, and 4.81 at 4.5, 28, and 38 GHz, respectively. As seen in V-V antenna polarization, the LOS PLE is 0.7 at 4.5 GHz and 0.92 at 28 GHz, both less than the theoretical free-space PLE of 2 and virtually identical at both frequencies, indicating that the indoor mmWave propagation channel experiences constructive interference from ground and ceiling bounce reflections and a waveguide effect down hallways and corridors that has a LOS directional PLE that is not frequency-dependent. For V-H antenna polarization, the LOS PLE in all frequencies is much greater than the LOS PLE in V-V antenna polarization, shown in Table 2. For NLOS environments, the 28 GHz PLE is 3.21 and 4.65 for V-V and V-H antenna polarization, respectively. And for 38 GHz, PLE is 4.38 and 5.28 for V-V and V-H antenna polarization, respectively. This indicates a significant depolarization effect in LOS and NLOS indoor environments at these frequencies. Table 2 shows the CI path loss model parameters for LOS and NLOS, at 4.5 GHz, 28 GHz, and 38 GHz.

The 38 GHz frequency band in LOS showed about 14 dB of attenuation per decade of distance values compared with the 28 GHz band, thereby proving that the sensitivity of the beam in future mmWave wireless systems, which measure TX-RX separation distances, was increased. The attenuation of NLOS (obstructed links) was approximately 15–23 dB greater than that of the unobstructed LOS links in all measured frequencies. The shadow factors of the mean path loss line for LOS V-V configuration were 3.14, 2.18, and 5.60 dB for the 4.5, 28, and 38 GHz bands, respectively. The 28 GHz and 38 GHz in V-H configuration LOS show a much larger shadow fading standard deviation that is approximately 8 dB and 13 dB for 28 GHz and 38 GHz compared with V-V

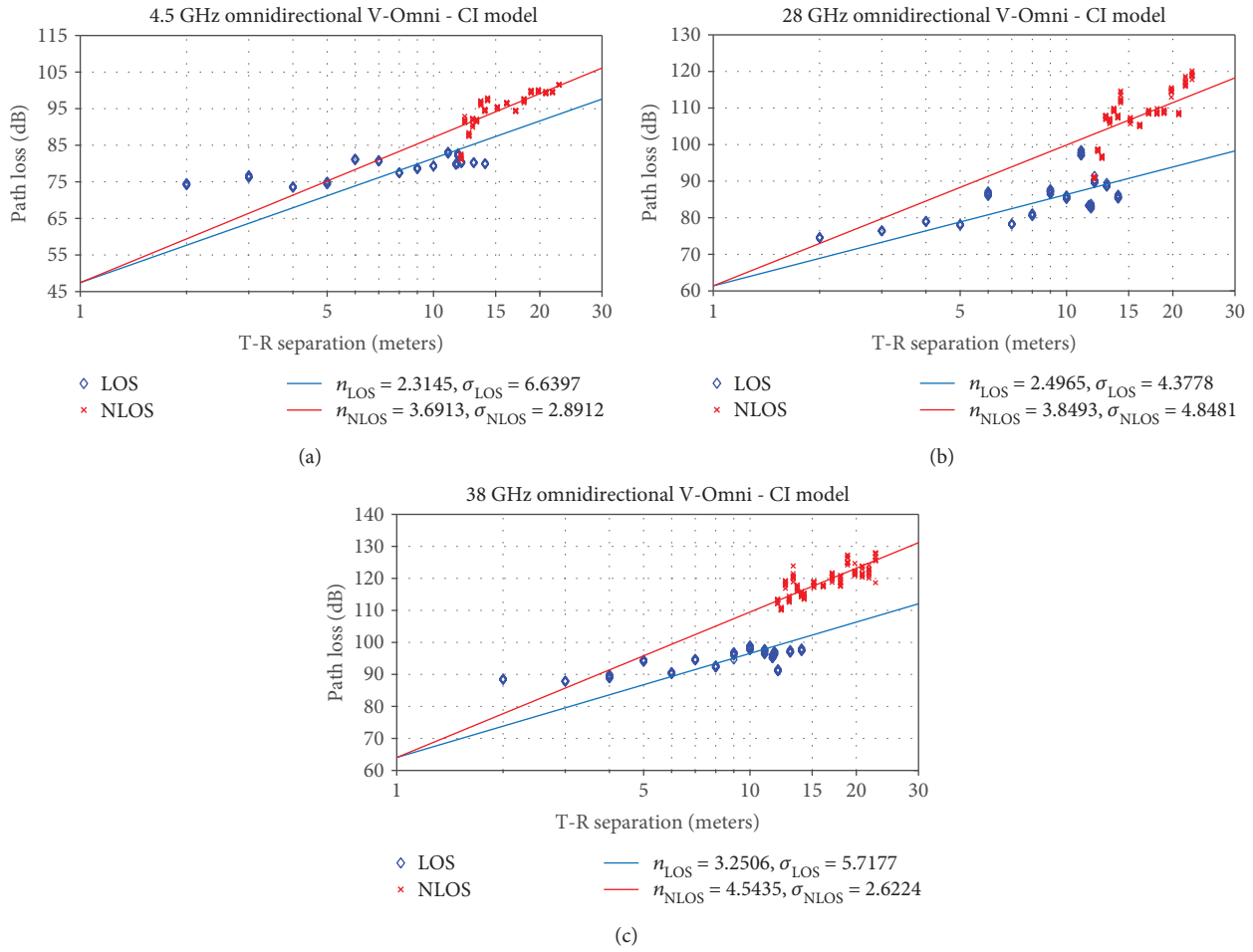


Figure 4: CI path loss model for omnidirectional V-Omni for LOS and NLOS (a) 4.5 GHz, (b) 28 GHz, and (c) 38 GHz.

Table 2: CI path loss model parameters for LOS and NLOS, at 4.5 GHz, 28 GHz, and 38 GHz.

| Frequency | Polarization | LOS | | NLOS | |
|---|---|---|---|---|---|
| | | PLE ($n$) | $\sigma$ (dB) | PLE ($n$) | $\sigma$ (dB) |
| 4.5 GHz | V-V | 0.70 | 3.14 | 2.26 | 4.56 |
| | V-H | 1.13 | 2.63 | 1.97 | 6.00 |
| | V-Omni | 2.31 | 6.64 | 3.69 | 2.89 |
| 28 GHz | V-V | 0.92 | 2.18 | 3.21 | 4.48 |
| | V-H | 3.87 | 7.83 | 4.65 | 3.57 |
| | V-Omni | 2.49 | 4.38 | 3.85 | 4.85 |
| 38 GHz | V-V | 2.29 | 5.60 | 4.38 | 4.14 |
| | V-H | 4.81 | 12.67 | 5.28 | 4.09 |
| | V-Omni | 3.25 | 5.72 | 4.54 | 2.62 |

configuration, indicating much larger fluctuations in received signal strength over all TX-RX separation distances. The standard deviations in V-V and V-Omni configurations for the LOS and NLOS measurements ranged from 2.2 dB to 6.6 dB among the studied frequencies, implying fewer fluctuations in the strongly received signal than in the average power received signal in all the TX-RX separation distances.

The FI path loss model results for the 4.5, 28, and 38 GHz frequency bands in LOS and NLOS environments are illustrated in Figures 5, 6, and 7 for (V-V), (V-H), and (V-Omni) antenna polarization, respectively. In LOS V-V, $\alpha$ values can vary compared with the free-space path losses, at 4.5 GHz it was 41.4 dB compared to the 45.5 dB theoretical FSPL at 1 m, at 28 GHz it was 60.1 dB compared to the 61.4 dB theoretical FSPL at 1 m, and it was 82.5 dB compared to the 64.0 dB theoretical FSPL at 1 m at the 38 GHz band. In LOS V-Omni, $\alpha$ values can vary compared with the free-space path losses, at 4.5 GHz it was 71.09 dB compared to the 45.5 dB theoretical FSPL at 1 m, at 28 GHz it was 68.23 dB compared to the 61.4 dB theoretical FSPL at 1 m, and it was 83.79 dB compared to the 64.0 dB theoretical FSPL at 1 m at the 38 GHz band. Table 3 shows the parameters for the FI path loss model.

The NLOS environment floating-intercept values were not frequency-dependent and varied from 16.2 dB to 87.9 dB. The slope values ($\beta$) of the mean least-square fit line were close to the free space ($\beta = 2$) in the NLOS environment for the 38 GHz band with co- and cross-polarized antennas, which does not necessarily imply that the NLOS signals afford much attenuation with distance than the free-space signals. The very low LOS $\beta$ slope values of 0.33 at 38 GHz

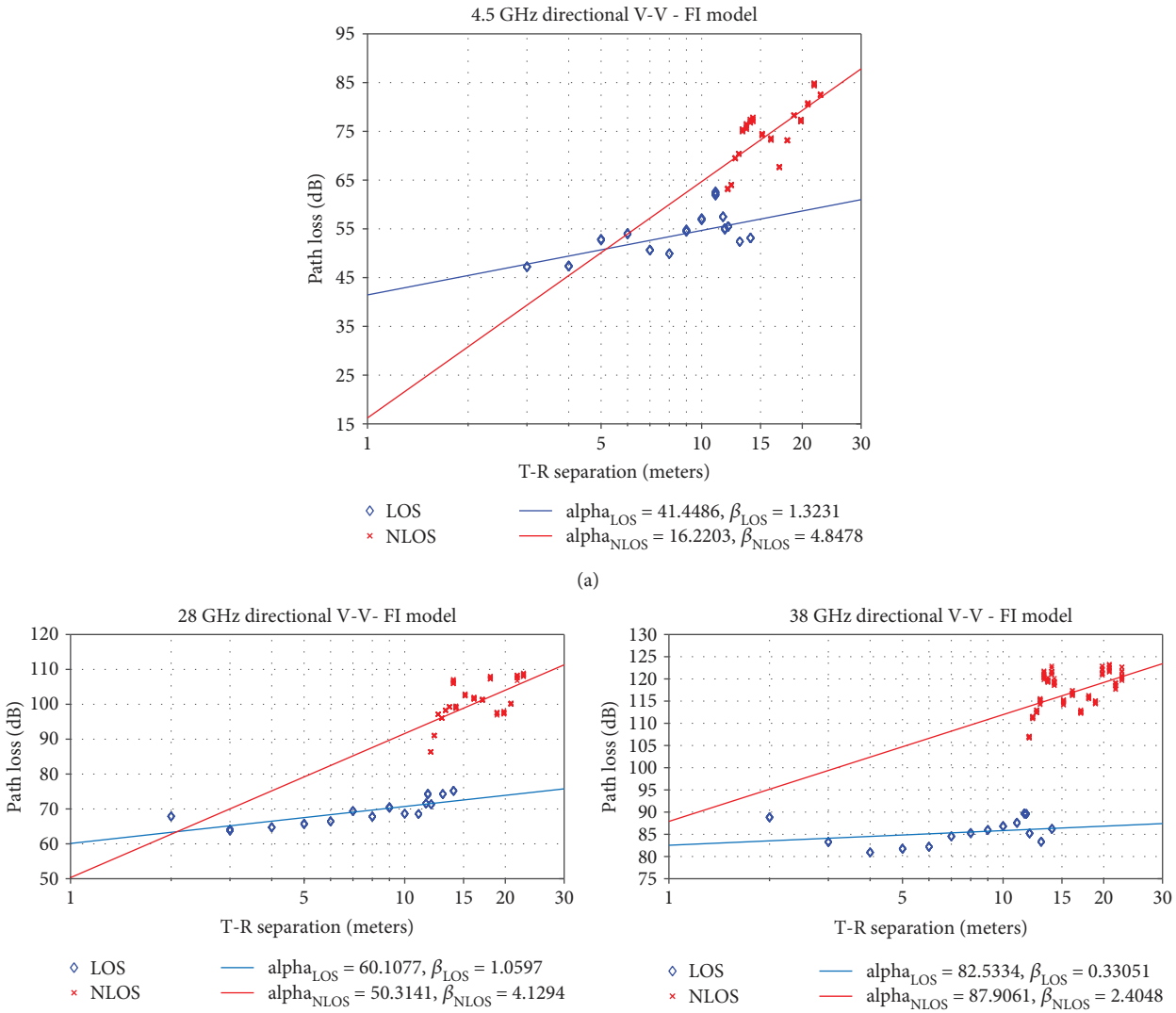


Figure 5: Directional V-V FI path loss model for LOS and NLOS (a) 4.5 GHz, (b) 28 GHz, and (c) 38 GHz.

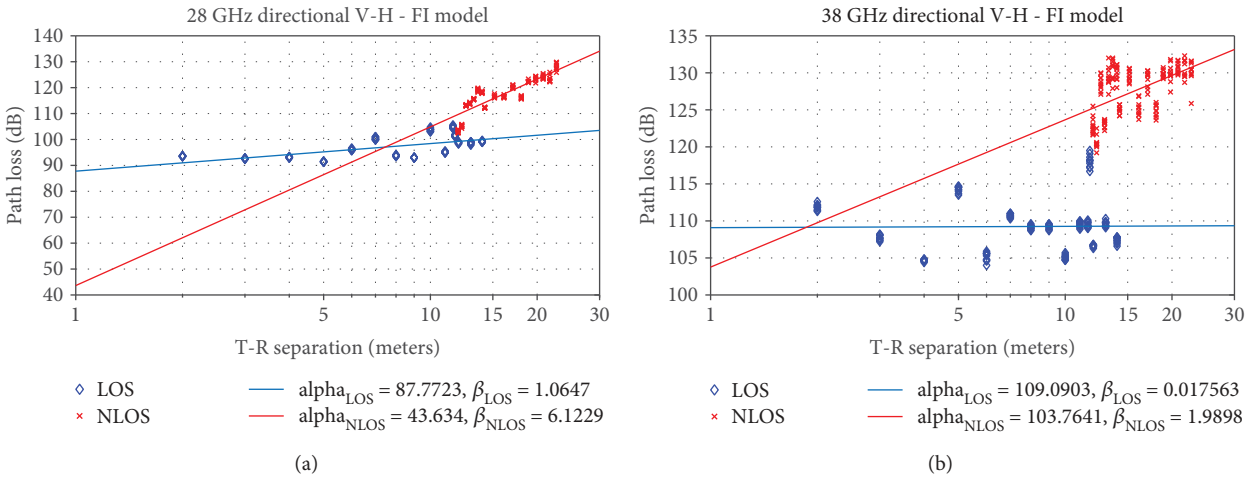


Figure 6: Directional V-H FI path loss model for LOS and NLOS (a) 28 GHz and (b) 38 GHz.

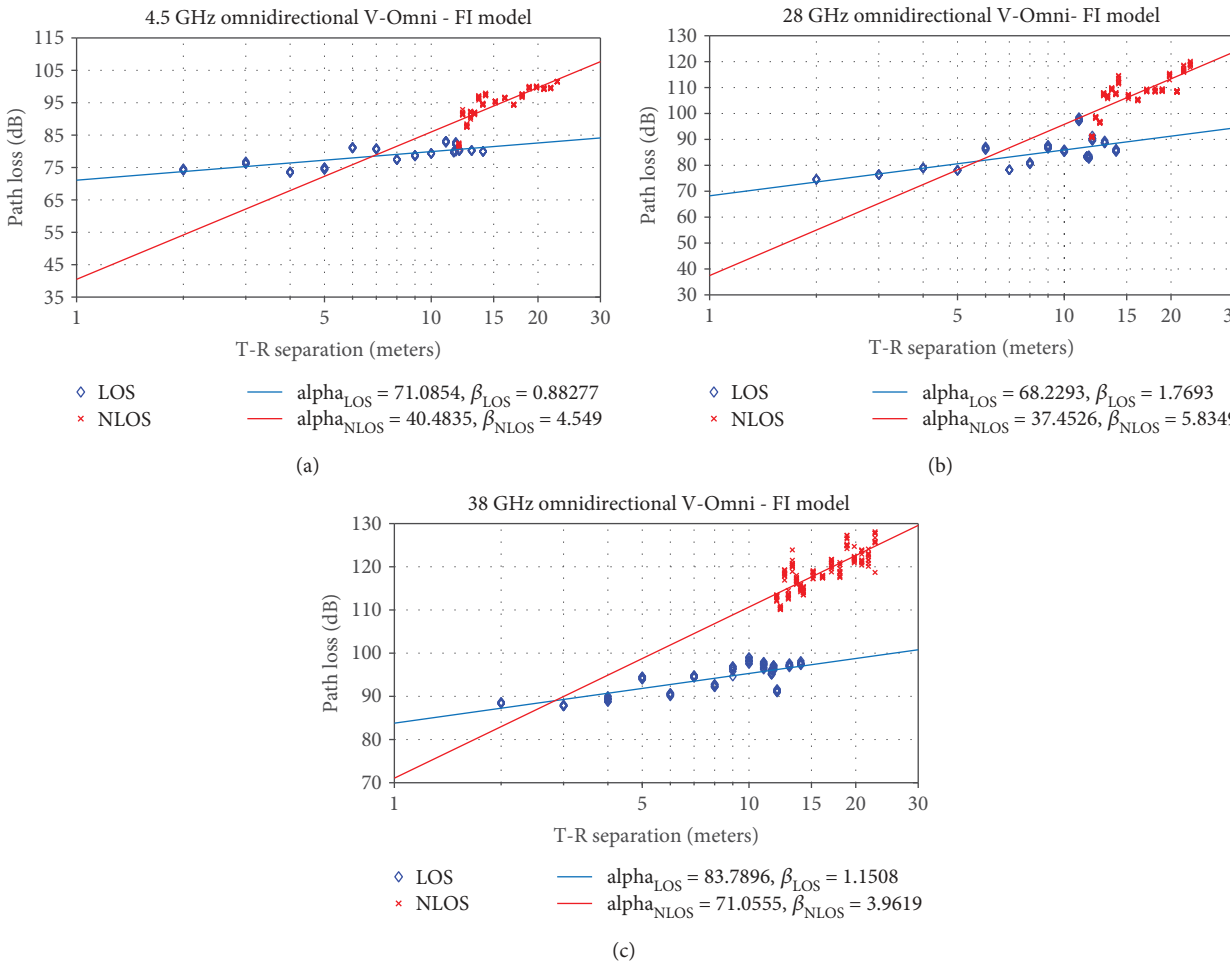


Figure 7: FI path loss model for omnidirectional V-Omni for LOS and NLOS (a) 4.5 GHz, (b) 28 GHz, and (c) 38 GHz.

Table 3: FI path loss model parameters for LOS and NLOS, at 4.5 GHz, 28 GHz, and 38 GHz.

| Frequency | Polarization | LOS | | | NLOS | | |
|---|---|---|---|---|---|---|---|
| | | $\alpha$ (dB) | $\beta$ | $\sigma$ (dB) | $\alpha$ (dB) | $\beta$ | $\sigma$ (dB) |
| 4.5 GHz | V-V | 41.45 | 1.32 | 1.79 | 16.22 | 4.85 | 3.91 |
| | V-Omni | 71.09 | 0.88 | 1.79 | 40.48 | 4.55 | 2.84 |
| 28 GHz | V-V | 60.10 | 1.06 | 2.15 | 50.31 | 4.13 | 4.39 |
| | V-H | 87.77 | 1.07 | 3.23 | 43.63 | 6.12 | 3.31 |
| | V-Omni | 68.23 | 1.77 | 3.97 | 37.45 | 5.83 | 4.50 |
| 38 GHz | V-V | 82.53 | 0.33 | 2.57 | 87.91 | 2.40 | 3.73 |
| | V-H | 109.09 | 0.01 | 3.48 | 103.76 | 1.99 | 2.81 |
| | V-Omni | 83.79 | 1.15 | 2.04 | 71.06 | 3.96 | 2.57 |

V-V and 0.01 for V-H antenna polarization show the extreme sensitivity of the FI model and how the model parameters defy physical interpretation (where PLE values of 0.33 and 0.01 indicate little increase in path loss as distance increases, which is unrealistic).

*7.2. Multifrequency Path Loss Model.* The ABG model is illustrated in Figures 8 and 9. It demonstrates the PL model for different frequencies, and it comprises distance- and frequency-dependent factors. Table 4 shows all ABG multi-frequency model parameters.

The distance dependence term $\alpha$ for the NLOS case study is higher by 33 and 39 dB/decades than that for the LOS case study for V-V and V-Omni, respectively, because of the absence of the direct path in the NLOS case study. The standard deviations of the ABG model for LOS and NLOS have a 0.01 difference in both polarizations. The frequency slopes ($\gamma$) are 4.83 and 5.81 for LOS and NLOS in the V-V case

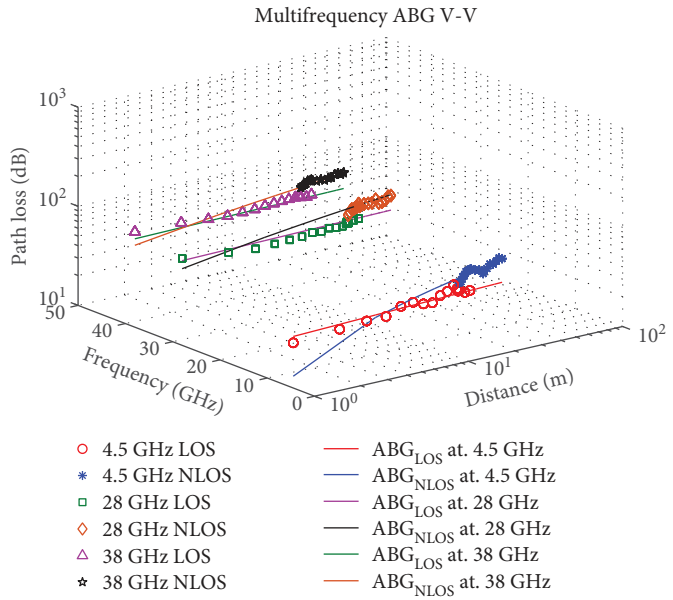


Figure 8: ABG model for directional V-V for LOS and NLOS at 4.5, 28, and 38 GHz.

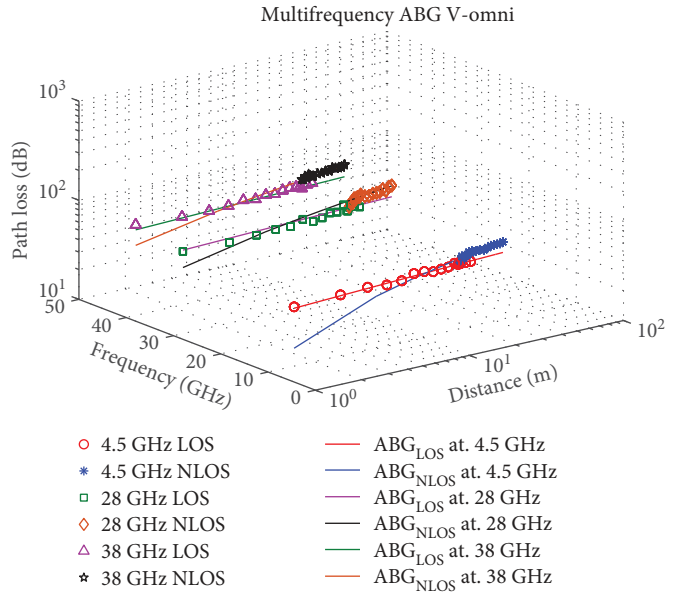


Figure 9: ABG model for omnidirectional V-Omni for LOS and NLOS at 4.5, 28, and 38 GHz.

Table 4: ABG model parameters for LOS and NLOS at 4.5, 28, and 38 GHz.

| 4.5, 28, and 38 GHz directional ABG model parameters | | | | | |
|---|---|---|---|---|---|
| Env. | Polarization | $\alpha$ | $\beta$ | $\gamma$ | $\sigma$ (dB) |
| LOS | V-V | 0.43 | 1.56 | 4.83 | 0.24 |
| | V-Omni | 0.90 | 35.77 | 3.02 | 0.19 |
| NLOS | V-V | 3.79 | −24.82 | 5.81 | 0.25 |
| | V-Omni | 4.81 | −3.67 | 3.91 | 0.18 |

study, and the frequency slopes ($\gamma$) are 3.02 and 3.91 for LOS and NLOS in V-Omni case study, respectively.

## 8. Proposed Model Analysis

The proposed model for the 28 GHz band in Figure 10 fits the measured data for the LOS and NLOS scenarios for V-V, V-H, and V-Omni antenna polarization, respectively. It only requires one parameter to be estimated, which is the correction factor for any environment. For the 38 GHz band, the large-scale path loss values are shown in Figure 11. The measurement data shows a slight difference between the path losses between different antenna polarizations in NLOS for

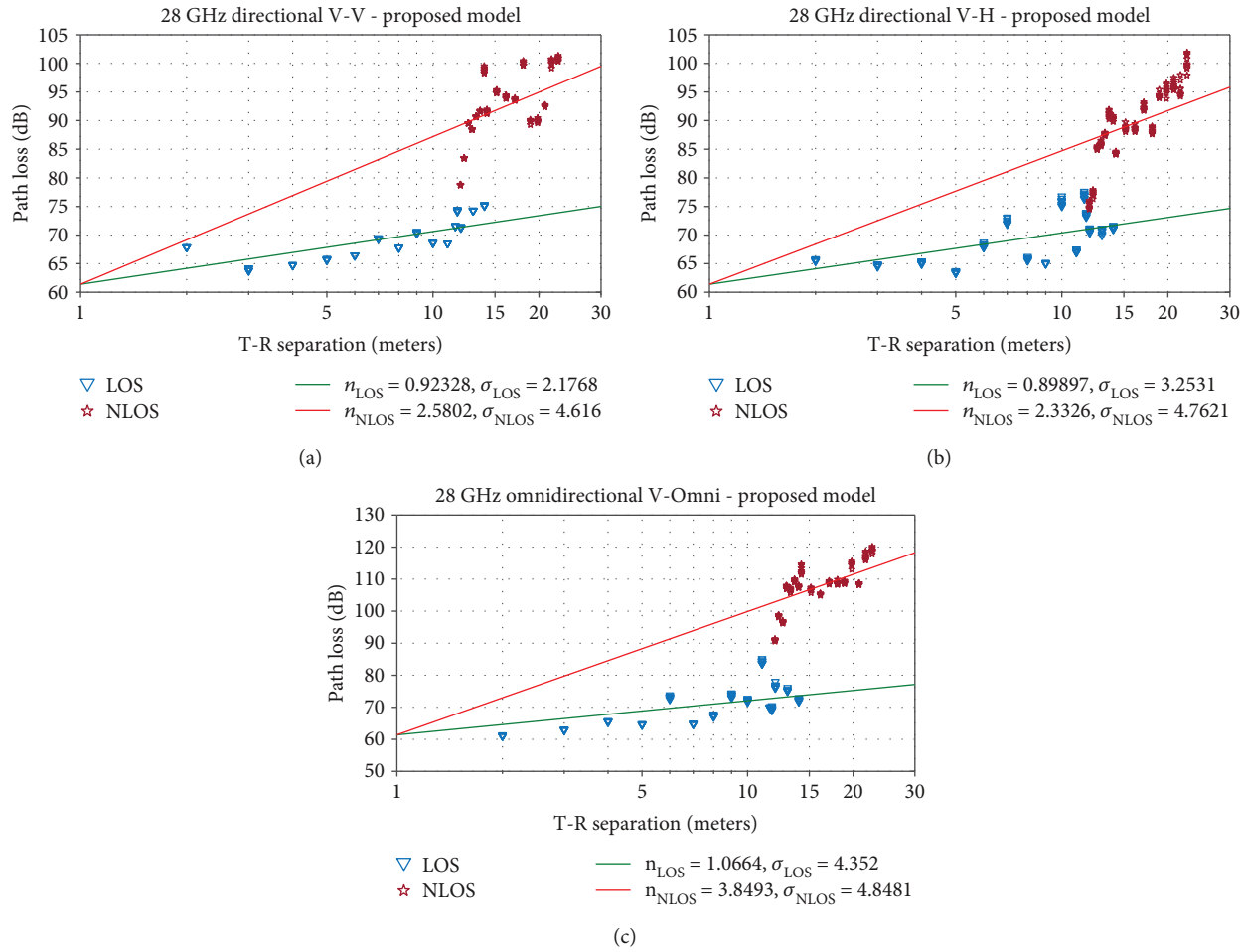


Figure 10: Proposed model for 28 GHz for LOS and NLOS (a) V-V, (b) V-H, and (c) V-Omni antenna polarization.

both frequency bands as shown in Table 5. The proposed model shows the same phenomena in the LOS scenario, where the path losses are extremely close to each other for both frequency bands. Hence, the proposed model is accurate and simple for the 28 GHz and 38 GHz bands. The proposed model PLEs in LOS 28 GHz are 0.92, 0.90, and 1.07 for V-V, V-H, and V-Omni antenna polarizations, respectively, and all values are less than theoretical FSPL 2 and less than PLEs compared with the CI path loss model, which have PLE 3.87 and 2.49 for V-H and V-Omni antenna polarizations, respectively.

As a comparison between the CI path loss model and the proposed model, in LOS 28 GHz, the PLE values for the proposed model are 0.92, 0.90, and 1.07 for V-V, V-H, and V-Omni antenna polarizations, respectively, compared to PLEs of 0.92, 3.87, and 2.49 for the CI path loss model for the same antenna polarizations. In LOS 38 GHz, the PLE values for the proposed model are 2.30, 2.24, and 2.40 for V-V, V-H, and V-Omni antenna polarizations, respectively, compared to PLEs 2.29, 4.81, and 3.25 for the CI path loss model for the same antenna polarizations.

In NLOS 28 GHz, the PLE values for the proposed model are 2.58, 2.33, and 3.85 for V-V, V-H, and V-Omni antenna polarizations, respectively, compared to PLEs 3.21, 4.65, and 3.85 for the CI path loss model for the same antenna polarizations. In NLOS 38 GHz, the PLE values for the proposed model are 4.23, 4.53, and 4.55 for V-V, V-H, and V-Omni antenna polarizations, respectively, compared to PLEs 4.38, 5.28, and 4.54 for the CI path loss model for the same antenna polarizations.

Also, most of the standard deviation $\sigma$ values for both frequencies in the proposed model show less values compared with standard deviation values for the CI path loss model. So, the proposed model shows better results in path loss prediction for PLE ($n$) and standard deviation $\sigma$ values for 28 GHz and 38 GHz in LOS and NLOS scenarios compared with the CI path loss model. Table 6 shows the comparison results between proposed and CI model parameters at the 28 GHz and 38 GHz frequency bands.

## 9. Conclusion

The large-scale path loss model for the indoor environment is presented in this paper for 4.5, 28, and 38 GHz bands. This measurement campaign was used to determine the effects of path loss when 5G signals are transmitted over these frequency bands. For the single-frequency path loss model, the CI model is more efficient in terms of measuring data than

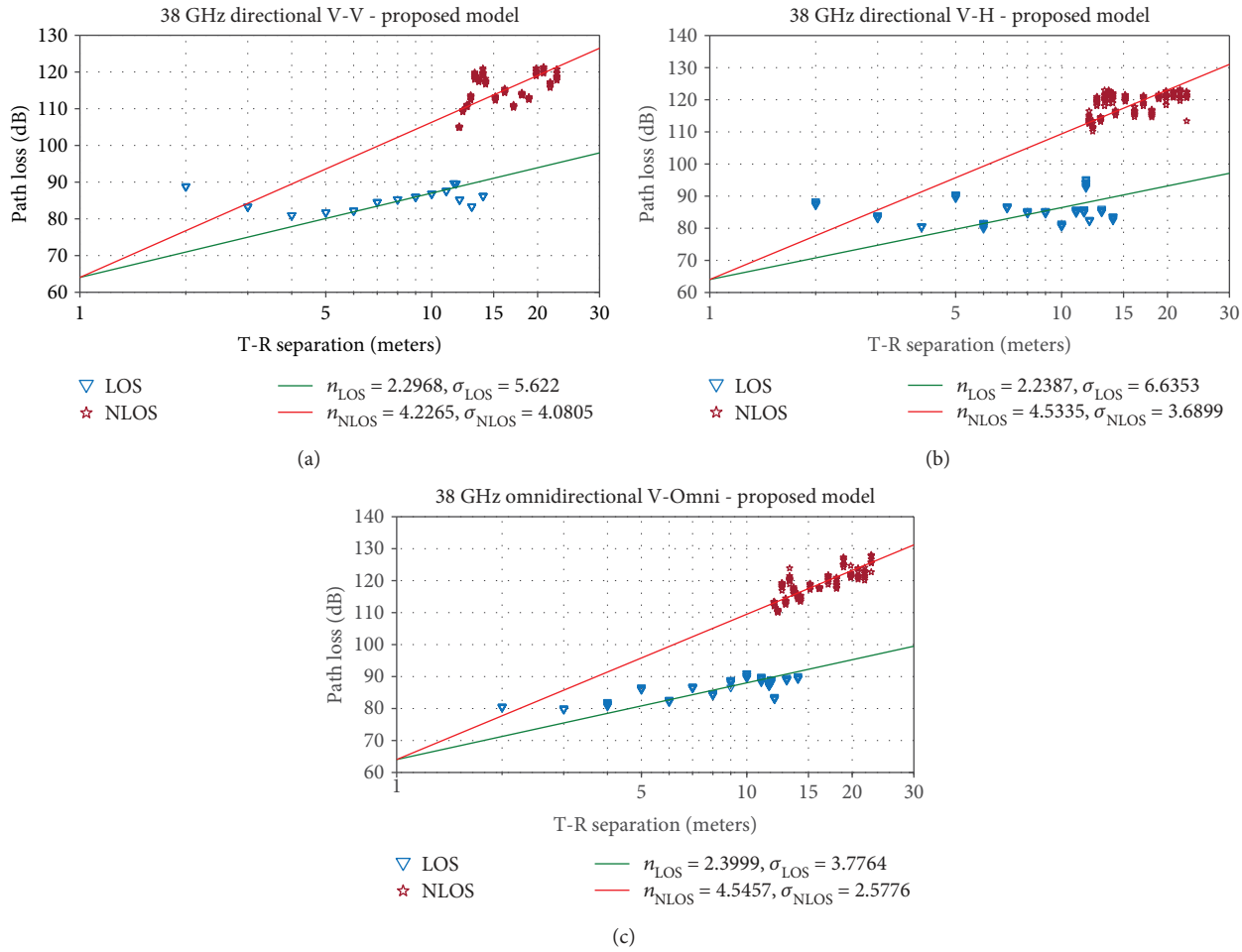


Figure 11: Proposed model for 38 GHz for LOS and NLOS (a) V-V, (b) V-H, and (c) V-Omni antenna polarization.

Table 5: Proposed model parameters for LOS and NLOS, at 28 GHz and 38 GHz.

| Frequency | Polarization | LOS | | NLOS | |
|---|---|---|---|---|---|
| | | $n^{Pro}$ | $\sigma^{Pro}$ (dB) | $n^{Pro}$ | $\sigma^{Pro}$ (dB) |
| 28 GHz | V-V | 0.92 | 2.18 | 2.58 | 4.62 |
| | V-H | 0.90 | 3.25 | 2.33 | 4.76 |
| | V-Omni | 1.07 | 4.35 | 3.85 | 4.85 |
| 38 GHz | V-V | 2.30 | 5.62 | 4.23 | 4.08 |
| | V-H | 2.24 | 6.64 | 4.53 | 3.69 |
| | V-Omni | 2.40 | 3.78 | 4.55 | 2.58 |

Table 6: Comparison between proposed and CI model's parameters for LOS and NLOS at 28 GHz and 38 GHz.

| Model | Frequency | Polarization | LOS | | NLOS | |
|---|---|---|---|---|---|---|
| | | | PLE ($n$) | $\sigma$ (dB) | PLE ($n$) | $\sigma$ (dB) |
| Proposed | 28 GHz | V-V | 0.92 | 2.18 | 2.58 | 4.62 |
| | | V-H | 0.90 | 3.25 | 2.33 | 4.76 |
| | | V-Omni | 1.07 | 4.35 | 3.85 | 4.85 |
| | 38 GHz | V-V | 2.30 | 5.62 | 4.23 | 4.08 |
| | | V-H | 2.24 | 6.64 | 4.53 | 3.69 |
| | | V-Omni | 2.40 | 3.78 | 4.55 | 2.58 |
| CI | 28 GHz | V-V | 0.92 | 2.18 | 3.21 | 4.48 |
| | | V-H | 3.87 | 7.83 | 4.65 | 3.57 |
| | | V-Omni | 2.49 | 4.38 | 3.85 | 4.85 |
| | 38 GHz | V-V | 2.29 | 5.60 | 4.38 | 4.14 |
| | | V-H | 4.81 | 12.67 | 5.28 | 4.09 |
| | | V-Omni | 3.25 | 5.72 | 4.54 | 2.62 |

the 3GPP models. The FI model results in highlighting the lack of sensitivity of the FI model in terms of reconciling the physical effects of environmental loss with distance. Therefore, the results indicate that the FI model does not physically represent the channel of the LOS or NLOS environment. The multifrequency ABG path loss model showed all frequency slope values ($\gamma$) in LOS and NLOS that represent an unrealistic amount of attenuation with increasing frequency. Also, the small difference in standard deviation suggests that the simpler, physical-based CI model could be more suitable for closed-form analysis compared with FI and ABG models. Also, the proposed model with a correction factor based on actual field power measurement campaigns was developed for both LOS and NLOS indoor

environments. Moreover, the proposed model when evaluated and compared with the CI, FI, and ABG models had demonstrated an average improvement from the other stated models, respectively; also, it proves that an acceptable communication link can be established on 28 and 38 GHz bands for indoor environments. Moreover, it can provide a sound estimation of the mmWave path loss as a function of distance and other environmental and system-specific parameters.

## Data Availability

All the data generated or analyzed in this study are available from the corresponding author on reasonable request.

## Conflicts of Interest

The authors declare that there are no conflicts of interest regarding the publication of this paper.

## Acknowledgments

This work is supported by the Ministry of Higher Education Malaysia and Universiti Teknologi Malaysia under Grant no. 4J209 and University of Malaya Research University Grant-Faculty Programme under Grant no. RF005A-2018.

## References

[1] J. D. Laster and J. H. Reed, "Interference rejection in digital wireless communications," *IEEE Signal Processing Magazine*, vol. 14, no. 3, pp. 37–62, 1997.

[2] H. G. Yoon, W. G. Chung, H. S. Jo, J. Lim, J. G. Yook, and H. K. Park, "Spectrum requirements for the future development of IMT-2000 and systems beyond IMT-2000," *Journal of Communications and Networks*, vol. 8, no. 2, pp. 169–174, 2006.

[3] R. J. Kerczewski and L. Jonasson, "Outcomes of the 2015 world radiocommunication conference for aeronautical spectrum and applications," in *2016 Integrated Communications Navigation and Surveillance (ICNS)*, Herndon, VA, USA, April 2016.

[4] Z. Pi and F. Khan, "An introduction to millimeter-wave mobile broadband systems," *IEEE Communications Magazine*, vol. 49, no. 6, pp. 101–107, 2011.

[5] Y. Li, J. Yang, and N. Ansari, "Cellular smartphone traffic and user behavior analysis," in *2014 IEEE International Conference on Communications (ICC)*, pp. 1326–1331, Sydney, NSW, Australia, June 2014.

[6] T. S. Rappaport, "Millimeter wave wireless communications: the renaissance of computing and communications," in *IEEE International Conference on Communications*, Sydney, June 2014.

[7] F. Aldhaban, "Exploring the adoption of smartphone technology: literature review," in *2012 Proceedings of PICMET '12: Technology Management for Emerging Technologies*, pp. 2758–2770, Vancouver, BC, Canada, July-August 2012.

[8] Gartner, "Gartner says by 2018, more than 50 percent of users will use a tablet or smartphone first for all online activities," 2014, http://www.gartner.com/newsroom/id/2939217.

[9] T. S. Rappaport, Shu Sun, R. Mayzus et al., "Millimeter wave mobile communications for 5G cellular: it will work!," *IEEE Access*, vol. 1, pp. 335–349, 2013.

[10] T. S. Rappaport, R. W. Heath Jr., R. C. Daniels, and J. N. Murdock, *Millimeter Wave Wireless Communications*, Prentice-Hall, Englewood Cliffs, NJ, USA, 2015.

[11] CISCO, "20 myths of Wi-Fi interference: dispel myths to gain high performing and reliable wireless," 2007, https://www.bradley.edu/dotAsset/887599c0-26bf-4be4-a5b9-3c0843b65d74.pdf.

[12] Z. Hays, G. Richter, S. Berger, C. Baylis, and R. J. Marks, "Alleviating airport WiFi congestion: an comparison of 2.4 GHz and 5 GHz WiFi usage and capabilities," in *Texas Symposium on Wireless and Microwave Circuits and Systems*, pp. 1–4, Waco, TX, USA, April 2014.

[13] C. Na, J. K. Chen, and T. S. Rappaport, "Hotspot traffic statistics and throughput models for several applications," in *IEEE Global Telecommunications Conference, 2004. GLOBECOM '04*, pp. 3257–3263, Dallas, TX, USA, November-December 2004.

[14] C. Na, J. K. Chen, and T. S. Rappaport, "Measured traffic statistics and throughput of IEEE 802.11b public WLAN hotspots with three different applications," *IEEE Transactions on Wireless Communications*, vol. 5, no. 10, pp. 3296–3305, 2006.

[15] C. Sergiou, P. Antoniou, and V. Vassiliou, "A comprehensive survey of congestion control protocols in wireless sensor networks," *IEEE Communications Surveys & Tutorials*, vol. 16, no. 4, pp. 1839–1859, 2014.

[16] M. Peng, C. X. Wang, F. Gao, and W. Xiang, "Advanced antenna technologies in the beyond IMT-advanced systems," *International Journal of Antennas and Propagation*, vol. 2013, Article ID 156831, 2 pages, 2013.

[17] M. Ur-Rehman, Q. H. Abbasi, A. Rahman, I. Khan, H. T. Chattha, and M. A. Matin, "Millimetre-wave antennas and systems for the future 5G," *International Journal of Antennas and Propagation*, vol. 2017, Article ID 6135601, 2 pages, 2017.

[18] H. Xu, V. Kukshya, and T. S. Rappaport, "Spatial and temporal characteristics of 60-GHz indoor channels," *IEEE Journal on Selected Areas in Communications*, vol. 20, no. 3, pp. 620–630, 2002.

[19] A. Maltsev, R. Maslennikov, A. Sevastyanov, A. Khoryaev, and A. Lomayev, "Experimental investigations of 60 GHz WLAN systems in office environment," *IEEE Journal on Selected Areas in Communications*, vol. 27, no. 8, pp. 1488–1499, 2009.

[20] T. S. Rappaport, J. N. Murdock, and F. Gutierrez, "State of the art in 60-GHz integrated circuits and systems for wireless communications," *Proceedings of the IEEE*, vol. 99, no. 8, pp. 1390–1436, 2011.

[21] R. C. Daniels, J. N. Murdock, T. S. Rappaport, and R. W. Heath, "60 GHz wireless: up close and personal," *IEEE Microwave Magazine*, vol. 11, no. 7, pp. 44–50, 2010.

[22] M. R. Akdeniz, Y. Liu, M. K. Samimi et al., "Millimeter wave channel modeling and cellular capacity evaluation," *IEEE Journal on Selected Areas in Communications*, vol. 32, no. 6, pp. 1164–1179, 2014.

[23] X. Zhou, Z. Zhong, B. Zhang et al., "Experimental characterization and correlation analysis of indoor channels at 15 GHz," *International Journal of Antennas and Propagation*, vol. 2015, Article ID 601835, 11 pages, 2015.

[24] S. E. Alexander, "Characterising buildings for propagation at 900 MHz," *Electronics Letters*, vol. 19, no. 20, p. 860, 1983.

[25] D. Akerberg, "Properties of a TDMA pico cellular office communication system," in *IEEE 39th Vehicular Technology Conference*, pp. 186–191, San Francisco, CA, USA, May 1989.

[26] A. A. M. Saleh and R. Valenzuela, "A statistical model for indoor multipath propagation," *IEEE Journal on Selected Areas in Communications*, vol. 5, no. 2, pp. 128–137, 1987.

[27] T. S. Rappaport and D. A. Hawbaker, "Effects of circular and linear polarized antennas on wideband propagation parameters in indoor radio channels," in *IEEE Global Telecommunications Conference GLOBECOM '91: Countdown to the New Millennium. Conference Record*, pp. 1287–1291, Phoenix, AZ, USA, December 1991.

[28] C. M. P. Ho, T. S. Rappaport, and M. P. Koushik, "Antenna effects on indoor obstructed wireless channels and a deterministic image-based wide-band propagation model for in-building personal communication systems," *International Journal of Wireless Information Networks*, vol. 1, no. 1, pp. 61–76, 1994.

[29] J. B. Andersen, T. S. Rappaport, and S. Yoshida, "Propagation measurements and models for wireless communications channels," *IEEE Communications Magazine*, vol. 33, no. 1, pp. 42–49, 1995.

[30] S. S. Ghassemzadeh, R. Jana, C. W. Rice, W. Turin, and V. Tarokh, "Measurement and modeling of an ultra-wide bandwidth indoor channel," *IEEE Transactions on Communications*, vol. 52, no. 10, pp. 1786–1796, 2004.

[31] T. S. Rappaport and S. Sandhu, "Radio-wave propagation for emerging wireless personal-communication systems," *IEEE Antennas and Propagation Magazine*, vol. 36, no. 5, pp. 14–24, 1994.

[32] H. Xu, V. Kukshya, and T. S. Rappaport, "Spatial and temporal characterization of 60 GHz indoor channels," in *Vehicular Technology Conference Fall 2000. IEEE VTS Fall VTC2000. 52nd Vehicular Technology Conference (Cat. No.00CH37152)*, pp. 6–13, Boston, MA, USA, September 2000.

[33] X. Wu, Y. Zhang, C. X. Wang, G. Goussetis, and M. M. Alwakeel, "28 GHz indoor channel measurements and modelling in laboratory environment using directional antennas," in *2015 9th European Conference on Antennas and Propagation (EuCAP)*, pp. 1–5, Lisbon, Portugal, May 2015.

[34] M. Lei, J. Zhang, T. Lei, and D. Du, "28-GHz indoor channel measurements and analysis of propagation characteristics," in *2014 IEEE 25th Annual International Symposium on Personal, Indoor, and Mobile Radio Communication (PIMRC)*, pp. 208–212, Washington, DC, USA, September 2014.

[35] H. Zhao, R. Mayzus, S. Sun et al., "28 GHz millimeter wave cellular communication measurements for reflection and penetration loss in and around buildings in New York City," in *2013 IEEE International Conference on Communications (ICC)*, pp. 5163–5167, Budapest, Hungary, June 2013.

[36] M. Peter, R. J. Weiler, W. Keusgen, T. Eichler, M. Kottkamp, and A. Nähring, "Characterization of mm-wave channel sounders up to W-band and validation of measurement results," in *2016 10th European Conference on Antennas and Propagation (EuCAP)*, pp. 1–5, Davos, Switzerland, April 2016.

[37] M. N. Hindia, A. M. Al-Samman, T. A. Rahman, and T. M. Yazdani, "Outdoor large-scale path loss characterization in an urban environment at 26, 28, 36, and 38 GHz," *Physical Communication*, vol. 27, pp. 150–160, 2018.

[38] S. Sun, G. R. MacCartney, and T. S. Rappaport, "Millimeter-wave distance-dependent large-scale propagation measurements and path loss models for outdoor and indoor 5G systems," in *2016 10th European Conference on Antennas and Propagation (EuCAP)*, pp. 1–5, Davos, Switzerland, April 2016.

[39] S. Deng, M. K. Samimi, and T. S. Rappaport, "28 GHz and 73 GHz millimeter-wave indoor propagation measurements and path loss models," in *2013 IEEE Global Communications Conference (GLOBECOM)*, pp. 1244–1250, London, UK, June 2015.

[40] G. R. Maccartney, T. S. Rappaport, S. Sun, and S. Deng, "Indoor office wideband millimeter-wave propagation measurements and channel models at 28 and 73 GHz for ultra-dense 5G wireless networks," *IEEE Access*, vol. 3, pp. 2388–2424, 2015.

[41] T. Abbas, F. Qamar, I. Ahmed, K. Dimyati, and M. B. Majed, "Propagation channel characterization for 28 and 73 GHz millimeter-wave 5G frequency band," in *2017 IEEE 15th Student Conference on Research and Development (SCOReD)*, pp. 297–302, Putrajaya, Malaysia, December 2017.

[42] F. Qamar, M. H. Siddiqui, K. Dimyati, K. A. Noordin, and M. B. Majed, "Channel characterization of 28 and 38 GHz MM-wave frequency band spectrum for the future 5G network," in *2017 IEEE 15th Student Conference on Research and Development (SCOReD)*, pp. 291–296, Putrajaya, Malaysia, December 2017.

[43] M. K. Samimi and T. S. Rappaport, "Statistical channel model with multi-frequency and arbitrary antenna beamwidth for millimeter-wave outdoor communications," in *2015 IEEE Globecom Workshops (GC Wkshps)*, pp. 1–7, San Diego, CA, USA, December 2015.

[44] D. Cassioli, M. Z. Win, and A. F. Molisch, "The ultra-wide bandwidth indoor channel: from statistical model to simulations," *IEEE Journal on selected areas in Communications*, vol. 20, no. 6, pp. 1247–1257, 2002.

[45] M. N. Hindia, T. A. Rahman, H. Ojukwu, E. B. Hanafi, and A. Fattouh, "Enabling remote health-caring utilizing IoT concept over LTE-femtocell networks," *PLoS One*, vol. 11, no. 5, article e0155077, 2016.

[46] T. S. Rappaport, G. R. MacCartney, M. K. Samimi, and S. Sun, "Wideband millimeter-wave propagation measurements and channel models for future wireless communication system design," *IEEE Transactions on Communications*, vol. 63, no. 9, pp. 3029–3056, 2015.

[47] A. M. Al-Samman, T. A. Rahman, M. H. Azmi, M. N. Hindia, I. Khan, and E. Hanafi, "Statistical modelling and characterization of experimental mm-wave indoor channels for future 5G wireless communication networks," *PLoS One*, vol. 11, no. 9, article e0163034, 2016.

[48] G. R. MacCartney, J. Zhang, S. Nie, and T. S. Rappaport, "Path loss models for 5G millimeter wave propagation channels in urban microcells," in *2013 IEEE Global Communications Conference (GLOBECOM)*, pp. 3948–3953, Atlanta, GA, USA, December 2013.

[49] S. Sun, T. S. Rappaport, T. A. Thomas et al., "Investigation of prediction accuracy, sensitivity, and parameter stability of large-scale propagation path loss models for 5G wireless communications," *IEEE Transactions on Vehicular Technology*, vol. 65, no. 5, pp. 2843–2860, 2016.